

Parallel grid library for rapid and flexible simulation development

Honkonen, I.^{a,b,*}, von Alfthan, S.^a, Sandroos, A.^a, Janhunen, P.^a, Palmroth, M.^a

^a*Finnish Meteorological Institute, Helsinki, Finland*

^b*Department of Physics, University of Helsinki, Helsinki, Finland*

Abstract

We present an easy to use and flexible grid library for developing highly scalable parallel simulations. The distributed cartesian cell-refinable grid (dccrg) supports adaptive mesh refinement and allows an arbitrary C++ class to be used as cell data. The amount of data in grid cells can vary both in space and time allowing dccrg to be used in very different types of simulations, for example in fluid and particle codes. Dccrg transfers the data between neighboring cells on different processes transparently and asynchronously allowing one to overlap computation and communication. This enables excellent scalability at least up to 32 k cores in magnetohydrodynamic tests depending on the problem and hardware. In the version of dccrg presented here part of the mesh metadata is replicated between MPI processes reducing the scalability of adaptive mesh refinement (AMR) to between 200 and 600 processes. Dccrg is free software that anyone can use, study and modify and is available at <https://gitorious.org/dccrg>. Users are also kindly requested to cite this work when publishing results obtained with dccrg.

Keywords: Parallel grid, adaptive mesh refinement, free open source software

PROGRAM SUMMARY

- 1
- 2 *Manuscript Title:* Parallel grid library for rapid and flexible simulation development
- 3 *Authors:* Honkonen, I., von Alfthan, S., Sandroos, A., Janhunen, P., Palmroth, M.

*Corresponding author.

E-mail address: ilja.honkonen@fmi.fi

Tel: +358503803147

Fax: +358295394603

Postal address: P.O. Box 503, 00101 Helsinki, Finland

4 *Program Title:* DCCRG
5 *Journal Reference:*
6 *Catalogue identifier:*
7 *Licensing provisions:* GNU LGPL v3
8 *Programming language:* C++
9 *Computer:* PC, Cluster, Supercomputer
10 *Operating system:* POSIX
11 *RAM:* 10 MB - 10 GB per process
12 *Number of processors used:* 1 - 32768 cores
13 *Supplementary material:*
14 *Keywords:* dccrg, parallel, grid, AMR, MPI, FVM, FEM
15 *Classification:* 4.12, 4.14, 6.5, 19.3, 19.10, 20
16 *External routines/libraries:* MPI-2 [1], boost [2], Zoltan [3], sfc++ [4]
17 *Nature of problem:*
18 Grid library supporting arbitrary data in grid cells, parallel adaptive mesh refinement,
19 transparent remote neighbor data updates and load balancing.
20 *Solution method:*
21 The simulation grid is represented by an adjacency list (graph) with vertices stored into a
22 hash table and edges into contiguous arrays. Message Passing Interface standard is used
23 for parallelization. Cell data is given as a template parameter when instantiating the grid.
24
25
26 *Restrictions:*
27 Logically cartesian grid.
28 *Additional comments:*
29
30 *Running time:*
31 Running time depends on the hardware, problem and the solution method. Small problems
32 can be solved in under a minute and very large problems can take weeks. The examples
33 and tests provided with the package take less than about one minute using default options.
34 In the version of dccrg presented here the speed of adaptive mesh refinement is at most of
35 the order of 10^6 total created cells per second.
36

37 **References**

- 38 [1] <http://www.mpi-forum.org/>
39 [2] <http://www.boost.org/>

- 40 [3] K. Devine, E. Boman, R. Heaphy, B. Hendrickson, C. Vaughan, Zoltan Data Manage-
41 ment Services for Parallel Dynamic Applications, *Comput. Sci. Eng.* 4 (2002) 90-97
42 doi:10.1109/5992.988653
- 43 [4] <https://gitorious.org/sfc++>

44 **1. Introduction**

45 During the rising phase of the solar cycle, it is becoming more important to
46 understand the physics of the near-Earth space. The dynamical phenomena caused
47 by the constant flow of magnetized collisionless plasma from the Sun creates
48 space weather that may have harmful effects on space-borne or ground-based tech-
49 nological systems or on humans in space. While the physics of space weather is
50 being studied with in situ instruments (e.g. NASA's Radiation Belt Storm Probes
51 launched in 2012-08-30¹) and by means of remote sensing, it is also important
52 to model the near-Earth space with numerical simulations. The simulations can
53 be used both as a context to the one-dimensional data sets from observations, as
54 well as a source to discover new physical mechanisms behind observed variations.
55 Present large scale (global) simulations are based on computationally light-weight
56 simplified descriptions of plasma, such as magnetohydrodynamics (MHD, [1],
57 [2], [3] and [4]). On the other hand the complexity and range of spatial scales
58 (from less than 10^1 to over 10^6 km) in space weather physics signifies the need to
59 incorporate particle kinetic effects in the modeled equation set in order to better
60 model, for example, magnetic reconnection, wave-particle interactions, shock ac-
61 celeration of particles, ring current, radiation belt dynamics and charge exchange
62 (see e.g. [5] for an overview). However, as one goes from MHD towards the full
63 kinetic description of plasma (from hybrid PIC [6] and Vlasov [7] to full PIC [8],
64 [9]), the computational demands increase rapidly, indicating that the latest high
65 performance computing techniques need to be incorporated in the design of new
66 simulation architectures.

67 As the number of cores in the fastest supercomputers increases exponentially
68 the parallel performance of simulations on distributed memory machines is be-
69 coming crucial. On the other hand, utilizing a large number of cores efficiently in
70 parallel is challenging especially in simulations using run-time adaptive mesh re-
71 finement (AMR). This is largely a data structure and an algorithm problem albeit

¹http://www.nasa.gov/mission_pages/rbsp/main/index.html

72 specific to massively parallel physical simulations running on distributed memory
73 machines.

74 In computer simulations dealing with, for example, continuous matter (a fluid)
75 the simulated domain is discretized into a set of points or finite volumes which we
76 will refer to as cells. At any given cell the numerical solution of a differential
77 equation describing the problem often depends only on data within a (small) part
78 of the simulated volume. This is true for a single time step in a solver for a
79 hyperbolic problem or a single iteration in a solver for an elliptic problem. This
80 spatial data dependency can be implemented implicitly in the solver function(s)
81 or explicitly as a separate grid library used by the application.

82 In a simple case the number of cells in the simulation stays constant and the
83 data dependency of each cell is identical allowing cell data to be stored in an
84 array whose size is determined at grid creation and the spatial neighbors to be
85 represented as indices into this array. A straightforward AMR extension of this
86 concept is to create additional nested grids in specific parts of the simulation do-
87 main with higher resolution. By solving each grid separately and interpolating the
88 results from finer grids into coarser grids one does not have to modify the solver
89 functions. This technique is used extensively for example by Berger (see [10] for
90 some of the earliest work) and by [11] and [12]. In the rest of this work however
91 we will concentrate on AMR implementations in which additional overlapping
92 grids are not created but instead cells of the initial grid are refined, i.e. replaced
93 with multiple smaller cells.

94 A generic unstructured grid (as provided for example by libMESH [13]) does
95 not admit as simple a description as above and is generally described by a directed
96 graph in which vertices represent simulation cells and directed edges represent the
97 data dependencies between cells. Unfortunately the nomenclature of graph theory
98 and geometry overlap to some extent and discussing both topics simultaneously
99 can lead to confusion. Figure 1 shows the nomenclature we use from this point
100 forward, the standard graph theoretical terms are given in parentheses for refer-
101 ence. A cell is a natural unit in simulations using the finite volume method (FVM)
102 and hereinafter we will use the term cell instead of vertex when discussing graphs.
103 Also an edge in FVM simulations usually refers to the edges of a cube represent-
104 ing the physical volume of a cell, and hence we will use the term arrow to refer
105 to a directed edge in a graph. Furthermore we note that each cell in the grid can
106 also represent, for example, a block of cells similarly to [3], but for the purposes
107 of this work the actual data stored in grid cells is largely irrelevant.

108 Since a graph can also be used to represent the cells and arrows of grids sim-
109 pler than an unstructured mesh, the question arises how does a particular program

Nomenclature

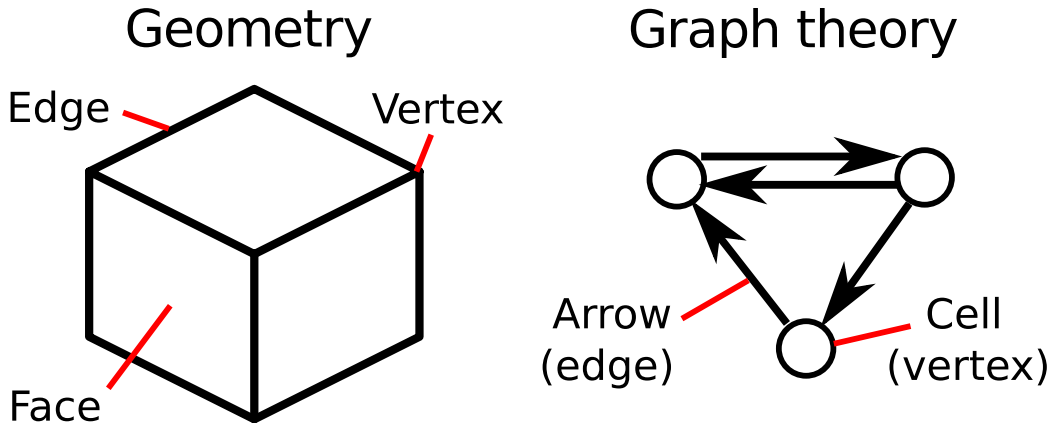


Figure 1: The nomenclature used in this work for geometry and graph theory. Standard graph theoretical terms are given in parentheses for reference.

110 implement its graph representation of the simulated system, e.g. what simplify-
111 ing assumptions have been made and how is the graph represented in memory.
112 A popular representation in (M)HD AMR simulations is to have a fixed number
113 of arrows directed away from each source cell and to store the arrows as native
114 pointers to the destination cells. In case a cell does not exist all arrows pointing to
115 it are invalidated in neighboring cells. This technique has been used with different
116 variations by [14], [15], [16] and [17], for example.

117 There are several possibilities for representing the cells and arrows of a graph,
118 for example an adjacency list or an adjacency matrix [18]. In physical simulations
119 the number of arrows in the graph is usually of the same order as the number of
120 cells in which case a suitable representation is an adjacency list. In an adjacency
121 list the cells of the graph are separate objects and each cell stores the arrows
122 pointing to and/or from that cell. The cells of the graph and the arrows of each
123 cell can be stored in different types of data structures. For example the cells are
124 stored in a contiguous array (representing a linear octree) in [19], [20], [21] and
125 [22], a hash table in [23] and a (doubly) linked list in [14]. On the other hand the
126 arrows of each cell are stored in a fixed size array of native pointers in [14] and as
127 single bits in [23].

128 In this work we introduce the distributed cartesian cell-refinable grid (dccrg)

129 for rapid development of parallel simulations using, for example, finite volume or
130 finite element methods (FEM). In dccrg the graph is represented by an adjacency
131 list in which cells are stored into a hash table, while the arrow lists of cells are
132 stored into contiguous arrays. We describe the details of the graph representation
133 in Section 2. In section 3 we describe the C++ implementation of dccrg and
134 present its unique features with respect to other published grid codes: arbitrary
135 data in grid cells, transparent updates of remote neighbor data, user-selectable
136 neighborhood size for cells and ease of use. In section 4 we test the scalability
137 of dccrg using a variety tests in one, two and three dimensions and draw our
138 conclusions in Section 5.

139 **2. Implementation of the grid graph**

140 Dccrg represents the grid as an adjacency list in which cells are stored into
141 a hash table. A hash table has one clear advantage over a tree when used to
142 store the grid: cells can be accessed, inserted and deleted in constant amortized
143 time regardless of the number of cells and their physical size and location. Thus
144 neither the total number of cells nor the number of refinement levels affect the
145 simulating performance of a single core. Each cell is associated with a unique id
146 which we use as a key into the hash table. A potential drawback of a hash table is
147 the computational cost of the hash function, but according to our tests the cost is
148 usually not important. The time to solve one flux between two cells in the MHD
149 tests presented in Section 4.1 is about four times larger than accessing one random
150 cell in the hash table. The cell access time can be optimized further, for example,
151 by storing and solving blocks of cells instead of single cells as is done in [3] and
152 discussed further in Section 3.1.1.

153 *2.1. Mapping cell ids to a physical location*

154 Our cell ids are globally unique integers which offers several advantages: 1)
155 The cell id can be calculated locally, i.e. without communication with other pro-
156 cesses, 2) The neighbors of a cell can be stored as cell ids instead of pointers that
157 are not consistent across computing nodes, 3) The cost of computing the hash
158 function values is minimized, 4) The memory required for storing the cell ids is
159 small.

160 Figure 2 shows an example of mapping cells to unique ids which is done as
161 follows: cell ids within each refinement level increase monotonically first in x
162 coordinate, then in y and then in z, with cells at refinement level 0 represented by
163 numbers from 1 to N_0 , refinement level 1 by numbers from $N_0 + 1$ to $N_0 + 1 + N_1$,

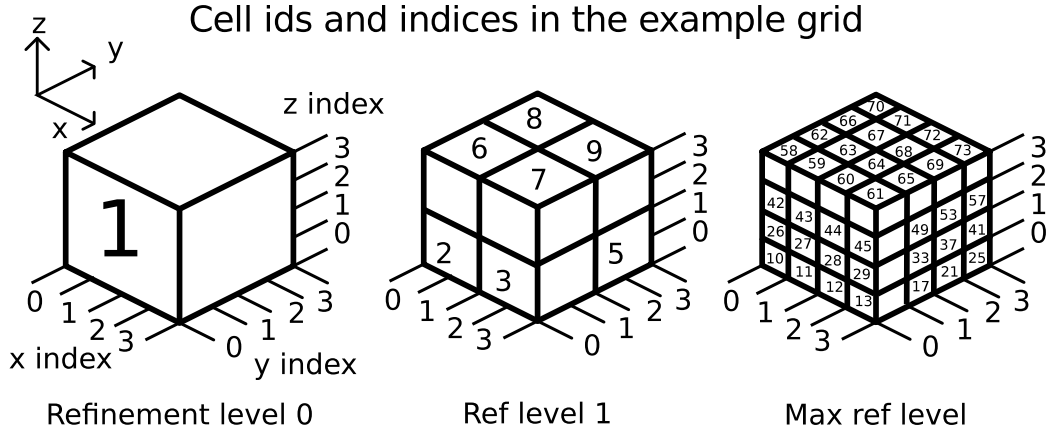


Figure 2: An example dccrg grid of size 1 in each dimension in cells of refinement level 0, with a maximum refinement level 2, showing the ids and indices of all possible cells.

164 etc. Cells at refinement level $l + 1$ are half the size of cells at refinement level l
 165 in each dimension. Cells at equal refinement level are identical in size. Hence in
 166 three dimensions $N_0 = \frac{N_1}{8} = \frac{N_2}{64} = \dots = n_x n_y n_z$, where n_x, n_y and n_z are the grid size
 167 in cells of refinement level 0 in the x, y and z dimensions respectively. Hereinafter
 168 cell size refers to the logical size of cells assuming a homogeneous and isotropic
 169 cartesian geometry.

170 When searching for the neighbors of a cell in the hash table (see Section 2.2)
 171 it is convenient to use the concept of cell indices: the location of each cell in the
 172 grid is represented by one number per dimension in the interval $[0, 2^L n_i - 1]$ where
 173 L is the maximum refinement level of the grid and n_i is n_x, n_y or n_z respectively.
 174 Figure 2 shows the possible cell indices for an example grid with $n_x = n_y = n_z = 1$
 175 and $L = 2$. The size of a single cell of refinement level l is 2^{L-l} indices in each
 176 dimension. A cell spanning more than one index is considered to be located at
 177 indices closest to the origin of the grid, for example cell #3 in Figure 2 is located
 178 at indices (2, 0, 0). Similarly to [24] there is a one-to-one mapping between cell
 179 ids and cell indices plus refinement levels, e.g. in addition to its id a cell can be
 180 uniquely identified by its indices and refinement level.

181 In the current implementation of dccrg a cell is refined by creating all of its
 182 children; in the example grid of Figure 2 refining cell #1 would create cells #2...#9.
 183 In principle this is not required and more complex grid structures are possible in
 184 which, for example, the grid in Figure 2 would consist of cells #1 and #3 alone.

185 Such an approach has been found useful by [14]. Complete refinement of cells in
186 our case was a practical decision based on our current simulation needs and it also
187 simplifies the neighbor searching code and enables optimizations described in the
188 next section.

189 2.2. Neighbor searching

190 In dccrg all cells existing within a certain minimum distance from local cells
191 (cells owned by the process) are stored in a hash table with the cell id as the key
192 and the process owning the cell as the value. Since the mapping of cell ids to a
193 location is unique, finding the neighbors of a cell in the hash table is straightfor-
194 ward: for all indices neighboring a given cell the hash table is searched for cells of
195 all applicable refinement levels. Figure 3 shows an example of neighbor searching
196 in a grid with $n_x = 2, n_y = n_z = 1, L = 3$ and a neighborhood size of one. The
197 siblings of cell #4 (#3, #7, #8, #11, #12, #15 and #16) are not shown for clarity
198 and some potential neighbors of cell #4 in the positive x direction have also been
199 omitted. In dccrg the cells' neighborhoods are measured in multiples of their own
200 size, e.g. for cell #4 all cells that are (at least partially) between indices 0 and
201 11 inclusive in the x direction would be considered as neighbors. In order to find
202 the neighbor(s) of cell #4 in positive x direction the hash table is searched for the
203 smallest cell at indices (8, 0, 0) which in this case could correspond to any of the
204 following cells: #2, #5, #23 or #155. If cell #23 is the smallest cell found in the
205 hash table the search can stop since it is known that the siblings of cell #23 also
206 exist (not shown, cells #24, #31, #32, #55, #56, #63 and #64) because all children
207 of a cell are created when a cell is refined. On the other hand if cell #155 is the
208 smallest cell found at indices (8, 0, 0) then the search would continue at indices
209 outside of cell #155 and its siblings, for example at indices (10, 0, 0) or (8, 2, 0).

210 The concept of hanging nodes or faces used in unstructured mesh codes is not
211 directly applicable to dccrg because a single cell is the smallest unit that dccrg
212 deals with. Since the user is responsible for defining what is stored in each cell
213 he/she must also define, if required, the data stored at the faces, edges and vertices
214 of cells. Hanging nodes, which are the result of cells of different size sharing an
215 edge or a face, must be handled by the solvers used for a particular application. For
216 example in GUMICS-4 [1] where the magnetic field is separated into background
217 and perturbed components the face average background magnetic field is required
218 when solving the flux through a face. With AMR a face average value of the
219 background field is required for every face of every cell because, for example, if
220 only one face average is stored per dimension in cells it would not be possible to
221 solve the flux between cells (#4, #2) and (#1, #5) in Figure 3. This is due to the

Neighbor searching

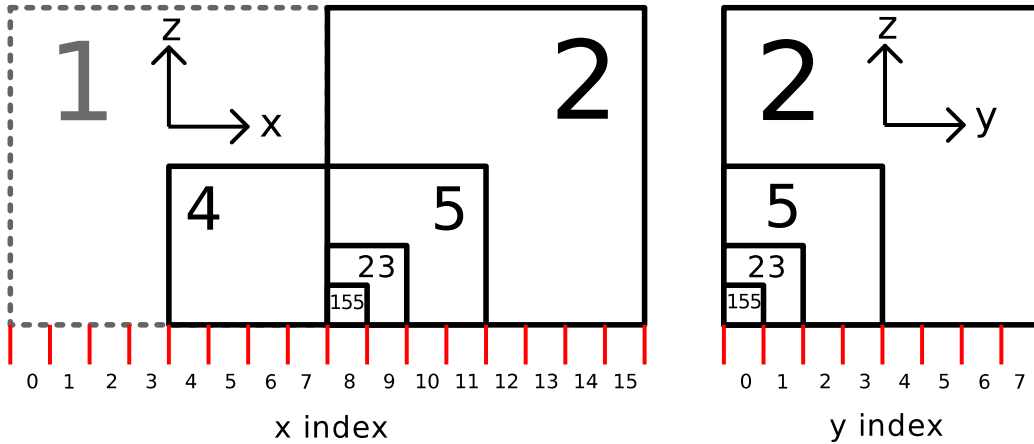


Figure 3: An example grid illustrating neighbor searching for cell #4 in the positive x direction. The siblings of cell #4 are not shown for clarity and also some of its potential neighbors in positive x direction have been left out.

222 fact that the face average value of the smaller cell must be used in both cases and
 223 it is only available if every face of every cell stores the face average field.

224 Currently dccrg enforces a maximum refinement level difference of 1 between
 225 neighboring cells. Hence it is sufficient to search for cells of three refinement
 226 levels $l - 1 \dots l + 1$ when finding the neighbors of a cell of refinement level l . In
 227 principle the enforcement of maximum refinement level difference is not required.
 228 For example in Figure 3 cell #4 (refinement level 1) has cell #155 (refinement level
 229 3) as a neighbor but in the current version of dccrg such a situation is not permitted
 230 and searching the hash table for cells #2, #5 and #23 is sufficient for finding the
 231 neighbors of cell #4. This was a practical decision based on our experience with
 232 global MHD modeling of the Earth's magnetosphere using GUMICS-4. In future
 233 this restriction might be removed. A similar one is also used in [24].

234 Even though a maximum refinement level difference of one is enforced be-
 235 tween neighboring cells and searching for cells in the hash table is a quick op-
 236 eration, in practice the ids of neighbors of local cells are also stored explicitly.
 237 As mentioned in Section 1, this neighbor information corresponds to arrows be-
 238 tween cells in a graph and hence we will use the term arrow list to refer to the
 239 neighbor list of a cell. Dccrg stores both the arrows pointing away from and the

240 arrows pointing to local cells. With AMR it is possible that there exists only one
241 arrow between two cells because cells' neighborhoods are measured in units of
242 their own size. For example in Figure 2 with a neighborhood size of 1, cell #13
243 would be considered a neighbor of cell #2 but cell #2 would not be considered a
244 neighbor of cell #13. Explicitly storing the arrows to and from local cells enables
245 fast iteration for example by user code (solvers, reconstruction functions, etc). In
246 dccrg the arrow lists of local cells are stored as contiguous arrays.

247 2.3. Algorithmic advantages

248 The most important advantage that globally unique cell ids have over a tradi-
249 tional graph implementation using native pointers between cells is that the arrows
250 between cells are not required to be consistent during AMR or load balancing.
251 For example when doing AMR, a pointer-based implementation has to be careful
252 not to leave any dangling pointers and to update the pointers of all nearby cells
253 in the correct order so as not to lose access to any cell. On the other hand with
254 unique cell ids the arrow lists of cells can simply be emptied when needed and
255 new neighbors searched in the hash table as described in Section 2.2. In addition
256 to being easy to implement this method also admits simple thread-based paral-
257 lelization inside dccrg due to different threads modifying only the arrow lists of
258 different cells.

259 It is also advantageous to use unique cell ids in arrow lists instead of pointers in
260 a parallel program running on distributed memory hardware. In this environment
261 a pointer to a neighboring cell is only valid on one process and cannot be used to
262 refer to the same neighbor on other processes. On the other hand the same unique
263 cell id can be used by all processes to refer to the same neighbor regardless of its
264 actual location in memory.

265 3. Implementation

266 A separate grid library is a natural abstraction probably for any physical sim-
267 ulation but especially for simulations using FVM where the concept of a grid and
268 its cells' data dependencies are easy to define and implement. Thus following
269 good software development practice dccrg is implemented independently of any
270 specific physical problem or its solver, while still providing the flexibility required
271 for various types of simulations, for example (M)HD, advection (e.g. Vlasov) and
272 kinetic.

273 Dccrg is written in C++ which allows us to easily separate low level function-
274 ality of dccrg into subclasses which higher-level classes can use thus also bene-

275 fitting from a modular internal implementation, a technique also used in [13]. For
276 example the physical geometry of the grid is handled by a separate class which is
277 also given to dccrg as a template parameter. This allows one to easily extend the
278 grid geometries supported by dccrg. In the default homogeneous and cartesian ge-
279 ometry cells of the same refinement level are identical in size in each dimension².

280 Here we describe the unique user-visible features of dccrg with respect to other
281 grid codes and also present important features of the serial and parallel implemen-
282 tation.

283 *3.1. Unique features*

284 *3.1.1. Arbitrary data in grid cells*

285 The most important feature distinguishing dccrg from other grid codes is the
286 possibility of trivially storing data of arbitrary type and size in the grid's cells
287 by simply giving the class which is stored in the cells as a template parameter to
288 dccrg when creating an instance of the grid. This also allows a single simulation
289 to have several independent parallel grids with different geometries and different
290 types of data stored in the grids' cells'. The amount of data can also vary between
291 different cells of the same grid and in the same cell as a function of time. This is
292 required for example in kinetic simulations where not only does the total number of
293 particles change but also the number of particles in each grid cell varies. In
294 dccrg this is handled by each instance of the user's cell data class providing a MPI
295 datatype corresponding to the data to be sent from or received by that particular
296 cell. An example of this is presented in Section 3.1.4.

297 Completely arbitrary cell data can also be transferred between processes if the
298 cell data class provides a serialize function which the MPI bindings of boost li-
299 brary will use for transferring cell data between processes³. Although this method
300 of transferring data between processes the most general it is also the slowest since
301 data is first copied into a contiguous buffer by serialization and subsequently trans-
302 ferred by MPI resulting in at least one additional copy the data being created com-
303 pared to pure a MPI transfer. This is also the case in the SAMRAI framework [25]
304 which supports transferring arbitrary patch data using the same technique.

305 *3.1.2. Automatic remote neighbor updates*

306 Dccrg can automatically transfer cell data between processes both for remote
307 neighbor data updates and load balancing using simple function calls. Further-

²https://gitorious.org/dccrg/dccrg/blobs/master/dccrg_constant_geometry.hpp

³User-defined data types in http://www.boost.org/doc/libs/1_49_0/doc/html/mpl/tutorial.html

308 more whenever cell data is sent between processes either one MPI message per
309 cell can be used or, similarly to [25], all cells being sent to another process can
310 be transferred using a single MPI message. Updating the remote neighbor data
311 between processes is possible using several methods. The simplest one is the
312 synchronous update function that updates the remote neighbor data between pro-
313 cesses and returns once transfers have completed (see Section 3.1.4). The most
314 fine-grained communication currently supported can be used by calling a separate
315 function for initiating transfers and functions that wait for the sends and receives
316 to complete respectively. A typical usage scenario would consist of the following:

- 317 1. Start transferring remote neighbor data
- 318 2. Solve the inner cells of the simulation (cells without remote neighbors)
- 319 3. Wait for the data from other processes to arrive
- 320 4. Solve the outer cells of the simulation (cells with at least one neighbor on
321 another process)
- 322 5. Wait for the data from this process to be sent

323 The MHD scalability tests we present in section 4.1 use this procedure with the
324 exception that step 5 is executed before step 4 due to the technical implementation
325 of the GUMICS-4 MHD solver.

326 *3.1.3. User-selectable neighborhood size*

327 As mentioned in Section 1 the size of cells' neighborhood in simulations is
328 highly problem / solver dependent. Specifically the problem / solver used in the
329 simulation dictates the distance from which data is required at a cell in order to
330 advance the simulation for one time step or one iteration in that cell. In many
331 previously published grid codes the size of cells' neighborhood is restricted to 1
332 either explicitly or implicitly. For example in [24] in three dimensions a block (a
333 single cell from the point of view of the grid) has 6 neighbors and it is assumed
334 that a block consist of such a number of simulation cells that, for example, a solver
335 needing data from a distance of 3 simulation cells can obtain that data from the
336 neighboring block. Other examples are [21], [19], [15], [13], [16] and [17]. Dc-
337 crg supports an arbitrarily large neighborhood chosen by the user when the grid is
338 initialized. The size of the neighborhood can be any unsigned integer and all other
339 cells within that distance of a cell (in units of size of the cell itself) will be consid-
340 ered as a neighbors of the cell. This enables the use of high-order solvers with the
341 added possibility of refining each neighboring cell individually. Naturally one can
342 also store a sufficiently large block of simulation cells in one dccrg cell allowing
343 one to use a small 6 cell neighborhood as done in [24]. Zero neighborhood size is

344 a special case in dccrg signifying that only face neighbors of equal size are con-
345 sidered neighbors (with AMR all of the refined neighbor's children are considered
346 instead). For example in a periodic grid without AMR neighborhood sizes of 1
347 and 2 would result in 26 and 124 neighbors per cell respectively.

348 Naturally the size of the neighborhood affects the amount of data that must be
349 transferred between processes during remote neighbor data updates regardless of
350 the grid implementation thus affecting parallel scalability. Additionally since in
351 dccrg a maximum refinement level difference of one is enforced between neigh-
352 boring cells the size of the neighborhood does affect for example the amount of
353 induced cell refinement (see Section 3.3).

354 *3.1.4. Ease of use*

355 Even though initially dccrg was developed only for in-house use, it was nev-
356 ertheless designed to be simple to use for the kinds of simulations it is targeted
357 for. Figure 4 shows an example of a complete parallel program playing Conway's
358 Game of Life using dccrg written in less that 60 lines of code (LOC) including
359 whitespace and comments. Lines 10...14 of the program define the class to be
360 stored in every cell of dccrg along with member functions `at` and `mpi_datatype`
361 which dccrg calls when querying the information required for transferring cell
362 data between processes. The current state of a cell is saved into `data[0]` and the
363 number of its live neighbors is saved into `data[1]`. On line 23 an instance of the
364 grid is created with the class defined above as `cell data`. On line 24 the geometry
365 of the grid is set to 10x10x1 cells at refinement level 0 with minimum coordinate
366 at (0, 0, 0) and cells of size 1 in each dimension. On line 25 the grid is initialized
367 by setting the load balancing function to use in Zoltan, the neighborhood size and
368 the maximum refinement level of cells. Lines 26 and 27 balance the load using
369 Zoltan and collect the local cells. In this example the load is balanced only once
370 and the local cell list does not change afterwards. On line 46 the non-existing
371 neighbors of local cells are skipped. This is because the grid is initialized with
372 non-periodic boundaries and neighbors that would be outside of the grid do not
373 exist.

374 Figure 5 shows relevant excerpts from a simple kinetic simulation showing the
375 use of dccrg in the case of variable amount of cell data, the full program can be
376 viewed in the dccrg git repository⁴. The remote neighbor update logic in the main
377 simulation loop consists of the following steps:

⁴<https://gitorious.org/dccrg/dccrg/blobs/master/tests/particles/simple.cpp>

- 378 1. The total number of particles in each cell is transferred between processes
379 (lines 43 and 44)
- 380 2. Space for receiving particle data is allocated in local copies of remote cells
381 based on their received total number of particles in step 1 (lines 47...52)
- 382 3. The particle coordinates are transferred between processes (lines 55 and 56)

383 The cell data class of the example kinetic simulation must provide the correct in-
384 formation to dccrg when updating remote neighbor data: The `at` and `mpi_datatype`
385 functions now return a different address and number of bytes respectively depend-
386 ing on whether the total number of particles or the particle coordinates are trans-
387 ferred between processes. This is decided by the user in the main simulation loop.
388 Additionally the `resize` function of the cell data class allocates memory for as
389 many particles as is there are in `number_of_particles`. A similar approach to
390 the one described above is also used in our Vlasov simulation (further developed
391 from [7]) where each real space cell has a separate adaptable velocity grid for ions
392 consisting of a variable number of 4^3 cell velocity blocks.

393 In the previous example two communications are required per time step be-
394 cause processes receiving particle data do not know the number of incoming par-
395 ticles in advance. Since the MPI standard requires that the maximum amount of
396 data to be received is known before calling the receive function the number of
397 particles has to be communicated separately. This guarantees that processes re-
398 ceiving particles can specify the size of the data to MPI and allocate the memory
399 required for received particles.

400 3.2. *Load balancing / cell partitioning*

401 Load balancing is also accomplished easily with dccrg. A user can call the
402 `balance_load` function to let the Zoltan [31] library create a new partition, and
403 single cells can also be moved manually between processes using the `pin` and
404 `unpin` functions. Most of Zoltan's load balancing methods⁵ can be used, namely:
405 NONE, RANDOM, BLOCK, RCB, RIB, HSFC, GRAPH, HYPERGRAPH and
406 HIER. In any case dccrg will transparently execute the new partition by transfer-
407 ring the necessary cell data between processes using MPI.

408 The structure of the grid in dccrg includes the owner of a cell in addition to the
409 unique id of the cell (id is the key and owner is the value in a hash table). Thus the
410 cell ids themselves are not used for partitioning cells between processes and any

⁵http://www.cs.sandia.gov/Zoltan/ug.html/ug_alg.html#LB_METHOD

411 cell can be moved to any process (for example by using the RANDOM partitioner
412 of Zoltan which we have found to be very useful for testing).

413 *3.3. Adaptive mesh refinement algorithm*

414 Due to the unique mapping of cells' ids and their physical location and size
415 it is straightforward to refine any given cell in the grid, i.e. to calculate the ids
416 of the children of any cell, and can be done locally (see Section 2). In order
417 to enforce a maximum refinement level difference of one between neighboring
418 cells whenever a cell is refined the refinement level of all neighbors is checked.
419 If the refinement level of any neighbor is less than that of the cell being refined
420 that neighbor is also refined. This is continued recursively until no more cells
421 need to be refined. The size of the cells' neighborhood affects induced refinement
422 indirectly by changing the number of neighbors a cell has and hence the potential
423 number of cells whose refinement will be induced. In dccrg a few simplifications
424 have been made to AMR: 1) Any set of cells can only be refined once before
425 calculating induced refinement (by `stop_refining`), e.g. induced refinement can
426 only increase the refinement level of cells by one, and 2) Unrefining a cell does not
427 induce unrefinement, e.g. any cell which has at least one neighbor with refinement
428 level larger than the cell being unrefined (i.e. it has a smaller neighbor) cannot be
429 unrefined.

430 In a parallel setting the only difference to the above is that whenever a process
431 refines or unrefines a cell that information has to be given to all processes which
432 have cells within a certain distance of the cell that was refined or unrefined. Cur-
433 rently this distance is equal to infinity, e.g. all changes to the structure of the grid
434 (refines and unrefines) are communicated globally. This has a significant impact
435 on the parallel scalability of AMR in dccrg and is discussed in Section 4 and a
436 method for making this minimum distance finite is discussed in Section 5. The
437 changes in grid structure are exchanged between processes after each recursive
438 step of induced refinement which are continued until no more cells need to be
439 refined.

440 *3.4. Parallel implementation*

441 Good scalability in distributed memory machines requires asynchronous point-
442 to-point MPI communication between processes with minimal total amount of
443 communication, and especially minimal amount of global communication. The
444 number of MPI messages should also be minimized in order not to burden the net-
445 work with unnecessary traffic. Therefore any process must know which processes

446 require data from local cells and from which remote cells data is required dur-
447 ing remote neighbor updates without querying that information from other pro-
448 cesses beforehand. Thus in dccrg every process knows the structure of the grid
449 (e.g. which cells exist and which processes own them) to at least a certain dis-
450 tance from any of its cells so it can calculate locally which cells' data to send and
451 receive from other processes. Due to this dccrg does not require global commu-
452 nication during ordinary time stepping, e.g. remote neighbor data updates, which
453 enables excellent scalability when not doing load balancing or AMR as shown
454 in section 4.1. Internally dccrg precalculates these send and receive lists when-
455 ever the structure of the grid changes due to AMR or cells being moved between
456 processes.

457 Even though the replicated mesh metadata of dccrg does not include the data
458 stored in each cell it nevertheless limits the size of dccrg grids in practice to less
459 than 100 M existing cells. This number does not depend on the refinement level
460 or physical location of the cells and has so far been more than sufficient for our
461 needs. To our knowledge the only parallel grid library that does not have any
462 persistent global data structures is [20]. In [21] and [22] only the macrostructure
463 of the grid (i.e. cells of refinement level 0) is known by all processes. According
464 to the authors this limits the size of the grid to the order of $10^5 \dots 10^6$ cells of
465 refinement level 0 but does not limit the number of smaller cells.

466 **4. Scalability results**

467 The time stepping scalability of dccrg (e.g. without AMR or load balancing)
468 depends mostly on the hardware running the simulation and on three parameters
469 specific to each simulated system: 1) the time required to solve the inner cells of a
470 process, 2) the amount of data transferred during the remote neighbor data update
471 of a process and 3) the time required to solve the outer cells of a process. We
472 show the dependency of dccrg scalability on these parameters by varying the total
473 number of cells and processes and by using a MHD solver in one, two and three
474 dimensions. The run-time AMR scalability of dccrg is also presented.

475 The non-AMR scalability tests were carried out on three different supercom-
476 puters: 1) A 2 k core Cray XT5m system with 12 core nodes connected by
477 SeaStar2 installed at the Finnish Meteorological Institute which we will refer to
478 as Meteo, 2) A 295 k core IBM Blue Gene/P system with 128 core nodes (node-
479 boards) installed at the Jülich Supercomputing Centre which we will refer to as
480 Jugene, and 3) A 12 k core bullx system with 32 core nodes connected by In-
481 finiBand installed at the Très Grand Centre de Calcul which we will refer to as

482 Curie.

483 *4.1. MHD tests without AMR*

484 First we show the time stepping scalability of dccrg in several MHD problems
485 with a solver developed for the global MHD model GUMICS-4 ([1]) which solves
486 ideal MHD equations in conservative form. Specifically the solver is a first order
487 Roe's approximate Riemann solver for a Godunov type problem [26]. In the test
488 results we present here only the Roe solver from GUMICS-4 is used as we do not
489 experience problems with negative pressures or densities in the presented tests.
490 The nature of the solver is such that when solving the flux through a face data
491 is only required from cells adjacent to the face, irrespective of the size of cells
492 involved. Thus interpolation of data is not required at any point in the solution
493 and if a cell has more than one face neighbor in any direction the flux through
494 each common face is solved in the usual way. In the tests presented here we do
495 not include a background magnetic field which is used in GUMICS-4 to represent
496 the Earth's dipole field.

497 The problems we use are the one-dimensional shock tube presented for exam-
498 ple in [27], the two-dimensional circularly polarized Alfvén wave presented by
499 [28] and further elaborated on by [29], and the three-dimensional blast wave pre-
500 sented by [30]. Periodic boundary conditions are used in all tests, except for the
501 shock tube test in the direction of the tube where initial conditions are enforced
502 after every time step. In MHD tests every cell contains the cell-averaged values of
503 the conservative MHD variables (density, momentum density, total energy density
504 and magnetic field) giving a total of 128 bytes which must be transferred when up-
505 dating the data of one cell between two processes. Since only the face neighbors
506 of a cell are required for calculating the next time step we use a neighborhood
507 size of zero in dccrg. In these tests processes execute one collective MPI com-
508 munication per time step in order to dynamically calculate the maximum physical
509 length of the time step. No other global communication is done. Since the grid is
510 static in these tests the computational load is balanced only once at the start of the
511 simulation by using a Hilbert space-filling curve⁶ instead of Zoltan.

512 Figure 6 shows the results of strong scalability tests using MHD with a static
513 grid in Meteo in one, two and three dimensions. The total number of cells (10 k,
514 50 k, 0.1 M, 0.5 M and 1 M) is kept constant while the number of MPI processes
515 is increased from 12 to 1536. In each test case scalability improves with the total

⁶<https://gitorious.org/sfc/sfc/blobs/master/sfc++.hpp>

516 number of cells because processes have more inner cells to solve while remote
517 neighbor data is being transferred. For example in the shock tube test every pro-
518 cess requires the data of two remote neighbors at most while the number of inner
519 cells with 1.5 k processes increases from about 4 (10 k total cells) to 649 (1 M
520 total cells). With 1 M cells the one and two dimensional tests scale almost ideally
521 in Meteo and the three dimensional test is also quite close to ideal. The overall
522 decrease in scalability with increasing number of dimensions is due to more data
523 being transferred between processes for the same number of local cells.

524 As suggested by the scalability results above most of the simulation time is
525 spent solving MHD which is shown in Figure 7 for the three dimensional blast
526 wave test using 1 M cells. The only global communication executed per time step
527 while simulating is the calculation of the maximum length of the physical time
528 step and is obtained using `MPI_Allreduce`. This is labeled as Allreduce in Figure
529 7 and basically shows the computational and MPI imbalance between processes
530 due to load balancing. Initialization and file I/O are not included in the profile and
531 other parts of the simulation take an insignificant fraction of the total run time.

532 The non-AMR scalability tests were also carried out in Jugene and Curie and
533 the results for the three-dimensional blast wave are shown in Figures 8 and 9
534 respectively. Similarly to Meteo the one and two dimensional tests (not shown)
535 scale better than the three-dimensional test in both Jugene and Curie. The overall
536 results are similar in all tested machines, e.g. scalability improves with increasing
537 number of total cells and decreasing number of dimensions. In Jugene very good
538 scalability up to 32 k processes is obtained for a total number of cells of 1 M and
539 above. The total simulation speed in Jugene is only slightly above that of Meteo
540 mostly due to the relatively small single-core performance of Jugene. Additionally
541 the average number of cells per process is more than 20 times larger in Meteo than
542 in Jugene for the maximum number of processes used but this has only a small
543 effect on scalability in Jugene.

544 In Curie good scalability up to 8 k processes is obtained only with 64 M total
545 cells but with a maximum solution speed of nearly 400 M solved cells per second
546 which is over twice of that in Jugene. We attribute this to the relatively low node
547 interconnect and high single-core and performance of Curie respectively when
548 compared to Jugene.

549 4.2. Scalability of run-time AMR

550 Figure 10 shows the speed of pure adaptive mesh refinement in dccrg. Initially
551 the grid is 8^3 , 16^3 , 64^3 or 128^3 cells and every process refines all local cells until
552 the total size of the grid is 128^3 or 256^3 cells. Initially the cells were partitioned

553 using a space-filling curve and this is not included in the timings. Cells also were
 554 not transferred between processes during AMR. As can be seen in Figure 10 the
 555 maximum cell refining speed of dccrg is of the order of 1 M cells per second. The
 556 linear scalability of AMR up to some 32 MPI processes is explained by the fact
 557 that after changes in the structure of the grid the arrow lists are recalculated only
 558 for local cells and MPI communication has not yet become a bottleneck. At 256
 559 processes the amount of global communication required for updating the structure
 560 of the grid between all processes starts to significantly affect the speed of AMR.
 561 This is discussed further in Section 4.3.

562 4.3. Scalability of blast wave test with AMR

Here we present the scalability of dccrg with AMR in the three-dimensional blast wave test used in Section 4.1. In this test a procedure similar to the one in GUMICS-4 (eq. 2 in [1]) is used to decide whether to refine or unrefine a cell: A refinement index is calculated for each cell based on the relative difference of several variables between a cell and its face neighbors. Here the calculation of refinement index α additionally includes velocity shear relative to the maximum wave velocity from the cells' interface. The full equation for the refinement index α is:

$$\alpha = \max\left(\frac{\Delta\rho}{\widehat{\rho}}, \frac{\Delta U_1}{\widehat{U}_1}, \frac{(\Delta p)^2}{2\rho\widehat{U}_1}, \frac{(\Delta B_1)^2}{2\mu_0\widehat{U}_1}, \frac{|\Delta B_1|}{\widehat{B}_1}, \frac{(\Delta v)^2}{v_{min}}\right)$$

563 where Δ denotes the difference in a variable between two cells, the hat denotes a
 564 minimum of the two values (as it actually does also in [1]), $v_{min} = \widehat{v}^2 + (0.01 \cdot v_{wave})^2$
 565 and v_{wave} is the maximum wave velocity from the cells' interface. In this test a cell
 566 is refined if $\alpha > 0.02 \cdot (l + 1)/L$, where l is the cell's current refinement level and
 567 $L = 4$ is the maximum refinement level of the grid. In other words a cell is
 568 refined to the maximum refinement level if its refinement index exceeds 0.02. A
 569 cell is unrefined if $\alpha < 0.02 \cdot (l + 1)/L/2$, e.g. a cell is kept at refinement level
 570 0 if $\alpha < 0.0025$ and none of the cell's neighbors' refinement levels exceed 1
 571 (due to dccrg enforcing a maximum refinement level difference of one between
 572 neighbors).

573 We use a maximum refinement level of 4 in this test with an initial grid of
 574 25^3 cells which results in an effective resolution of $400^3 = 64$ M cells. The com-
 575 putational load is balanced using Zoltan's recursive coordinate bisection (RCB)
 576 algorithm whenever the fraction of local cells ($f_c = N_{max}/N_{min}$, where max and
 577 min are the maximum and minimum number of local cells among all processes
 578 respectively) exceeded a specified limit. Animation 1 (Figure 11 in the print ver-
 579 sion) shows from left to right, top to bottom the grid, pressure, magnetic and

580 kinetic energy density during the simulation (at the end of the simulation in print
581 version) in the $y = 0$ plane when grid is adapted at every time step. At the end
582 of the simulation the fraction of maximum to minimum values are 15 for density
583 (not shown), 43 for pressure and 2.3 for magnetic energy density. Even though
584 the MHD solver we use is simpler than the one in [30] the results are still close
585 due to the high effective resolution achieved by using run-time AMR.

586 Figure 12 shows the total solution speed during the simulations as a function of
587 the number of MPI processes used. In the reference run a CFL [34] of 0.4 is used,
588 AMR is done at every time step and the load is balanced whenever the local cell
589 fraction $f_c \geq 2$. The AMR_N runs are otherwise identical to the reference run but
590 CFL is set to $0.4/N$ and AMR is done every N th time step, essentially multiplying
591 the amount of non-AMR work in these runs by N . The results between different
592 AMR runs are identical by visual inspection except for increased diffusion in runs
593 with low CFL. The ratio of work required by AMR and the rest of the simulation
594 has a significant effect on the total solution speed. The solution speed is a factor
595 of 5 higher in the AMR_{32} run than in the reference run when using about 500 MPI
596 processes. In the reference AMR run the total solution speed is close to 1/10 of
597 the non-AMR version with up to 144 processes and in the AMR_{32} the speed is
598 close to 1/3 with up to 288 processes after which both fractions start to decrease.
599 We define these as the regions of excellent AMR scalability. On the other hand
600 in all of the AMR runs the total solution speed increases up to about 500 to 600
601 processes after which it starts to decrease. We define this as the region where
602 AMR is scalable. The total number of cells in the AMR runs averages to 4.5
603 M which is about 1/14 of the non-AMR version. Consequently in the region of
604 excellent scalability the time to solution when using AMR is about 67 % to 22 %
605 of the non-AMR time for the reference and AMR_{32} runs respectively. Even with a
606 higher number of MPI processes it can still be advantageous to use AMR because
607 the number of simulation cells is over a magnitude lower than without AMR. At
608 the end of the AMR runs 9.9 M cells exist in the grid and the total number of
609 cells created and removed is between 40.2 M and 40.7 M, depending mostly on
610 the diffusion, and averages to about 91 k added + removed cells per time step.

611 Figure 13 shows which parts of the AMR blast wave test require the most
612 time. As the number of processes is increased the largest fraction of simulation
613 time is spent in global communication related to AMR and load balancing. The
614 Allreduce label again indicates global calculation of the physical time step and the
615 Load balancing label indicates the simulation time spent in load balancing related
616 functions. At about 300 MPI processes and above the largest fraction of simu-
617 lation time is spent communicating changes in the structure of the grid between

618 all processes. This includes both refining and unrefining cells as well as load bal-
619 ancing and in each case the `MPI_Allgatherv` function is used for distributing the
620 changes in grid structure between all processes. Only a small fraction of the time
621 spent in load balancing related functions is taken by Zoltan.

622 **5. Discussion**

623 While the ease of use of a software library is subjective it can be quantified
624 by the number of lines of code required for usage and compared against other
625 libraries when using the same programming language. With `dccrg` a complete
626 parallel program playing Conway's game of life can be implemented in less than
627 60 LOC including whitespace and comments. Even though the required LOC
628 is a crude estimate for a software library's ease of use it is nevertheless telling
629 that such a short parallel program does not seem to be possible with other grid
630 libraries.

631 The flexibility of `dccrg` also stands out since as far as we know only [25] al-
632 lows one to easily exchange arbitrary cell data between MPI processes. Addition-
633 ally `dccrg` supports transferring user-defined MPI datatypes which is critical for
634 performance in some applications. For example when solving the 6 dimensional
635 Vlasov equation in the Earth's magnetosphere ([7]) the simulation is heavily mem-
636 ory bound and using MPI datatypes directly for exchanging remote neighbor data
637 is significantly faster than serializing said data into an additional buffer(s) before
638 transfer. `Dccrg` also provides automatic neighbor data updates between processes
639 with the ability of easily overlapping computation with communication.

640 Currently the largest drawback of `dccrg` is the fact that the entire structure of
641 the grid is known by every process, i.e. a part of the mesh metadata is replicated
642 by all processes. The global data structure prevents grids larger than about 100 M
643 cells but this has not been a problem for us and can be worked around by storing
644 blocks instead of single cells into `dccrg` (similarly to [14], for example). The
645 global grid data structure of `dccrg` also reduces the scalability of AMR in the worst
646 case to about 200 and overall to about 600 MPI processes. Nevertheless using
647 AMR can lead to significant savings in the required memory as the number of cells
648 can be one or even two orders of magnitude lower. Depending on the problem the
649 required CPU time can also be significantly reduced when using AMR especially
650 when the number of MPI processes used is of the order of 300 or less. It should
651 also be noted that using threads to parallelize solvers within a shared memory
652 node could effectively multiply the scalability range of simulations by the number
653 of cores within one node, but this was not investigated.

654 Removing or significantly reducing the global data structure (as done in [20],
655 [21] and [22]) should improve both the largest attainable grid size and scalability
656 of AMR considerably. Intuitively this is straightforward since with the exception
657 of load balancing every process only needs to know the structure of the grid up to
658 some finite distance from local cells. In order to be able to arbitrarily refine and
659 unrefine grid cells without global communication local changes in the structure
660 of the grid must be communicated between all neighboring processes. A neigh-
661 boring process is defined as any process that has one or more of its cells inside
662 the neighborhood of any cell of refinement level 0 that overlaps a local cell. In
663 other words if only level 0 cells exist in the grid then the owners of all remote
664 neighbors of local cells are considered as neighboring processes; and this holds
665 no matter how the grid is subsequently refined and unrefined assuming that cells
666 are not transferred between processes (load balancing). Global communication
667 can also be avoided during load balancing if, for example, cells can be transferred
668 only between neighboring processes. Even in this case new neighbor processes
669 have to be recalculated but global communication is not required because cells
670 could only have been transferred to/from a subset of all processes. Implementing
671 this completely distributed mesh metadata is left to a subsequent study.

672 We presented the distributed cartesian cell-refinable grid (dccrg): an easy to
673 use parallel structured grid library supporting adaptive mesh refinement and ar-
674 bitrary C++ classe as cell data. Various MHD scalability results were presented
675 and depending on the problem, hardware and whether AMR is used excellent to
676 average scalability is achieved. Dccrg is freely available for anyone to use, study
677 and modify under version 3 of the GNU Lesser General Public License and can
678 be downloaded from <https://gitorious.org/dccrg>.

679 **6. Acknowledgements**

680 This work is a part of the project 200141-QuESpace, funded by the Euro-
681 pean Research Council under the European Community's seventh framework pro-
682 gramme. The research leading to these results has also received funding under
683 grant agreement no 260330 of the European Community's seventh framework
684 programme. IH and MP are supported by project 218165 and AS is supported
685 by project 251797 of the Academy of Finland. Results in this paper have in part
686 been achieved using the PRACE Research Infrastructure resource Curie based in
687 France at TGCC and Jugene based in Germany at JSC. IH thanks Daldorff, L.K.S.
688 and Pomoell, J. for insightful discussions.

689 **References**

- 690 [1] P. Janhunen, M. Palmroth, T. Laitinen, I. Honkonen, L. Juusola, G.
691 Facskó, T.I. Pulkkinen, The GUMICS-4 global MHD magnetosphere-
692 ionosphere coupling simulation, *J. Atmos. Sol.-Terr. Phys.* 80 (2012) 48-59
693 doi:10.1016/j.jastp.2012.03.006
- 694 [2] J.G. Lyon, J.A. Fedder, C.M. Mobarry, The Lyon-Fedder-Mobarry (LFM)
695 global MHD magnetospheric simulation code, *J. Atmos. Sol.-Terr. Phys.* 66
696 (2004) 1333-1350 doi:10.1016/j.jastp.2004.03.020
- 697 [3] K.G. Powell, P.L. Roe, T.J. Linde, T.I. Gombosi, D.L. De Zeeuw, A
698 Solution-Adaptive Upwind Scheme for Ideal Magnetohydrodynamics, *J.*
699 *Comput. Phys.* 154 (1999) 284-309 doi:10.1006/jcph.1999.6299
- 700 [4] J. Raeder, R.J. Walker, M. Ashour-Abdalla, The structure of the distant geo-
701 magnetic tail during long periods of northward IMF, *Geophys. Res. Lett.* 22
702 (1995) 349-352
- 703 [5] H.E.J. Koskinen, *Physics of Space Storms: From the Solar Surface to the*
704 *Earth*, Springer-Verlag (2011) doi: 10.1007/978-3-642-00319-6
- 705 [6] E. Kallio, P. Janhunen, Modelling the solar wind interaction with Mer-
706 cury by a quasi-neutral hybrid model, *Ann. Geophys.* 21 (2003) 2133-2145
707 doi:10.5194/angeo-21-2133-2003
- 708 [7] M. Palmroth, I. Honkonen, A. Sandroos, Y. Kempf, S. von Alfthan, D.
709 Pokhotelov, Preliminary testing of global hybrid-Vlasov simulation: Magne-
710 tosheath and cusps under northward interplanetary magnetic field, *J. Atmos.*
711 *Sol.-Terr. Phys.* accepted (2012)
- 712 [8] C.K. Birdsall, A.B. Langdon, *Plasma Physics via Computer Simulation*,
713 McGraw-Hill Book Co. (1985)
- 714 [9] R.W. Hockney, J.W. Eastwood, *Computer Simulation Using Particles*, Adam
715 Hilger (1988)
- 716 [10] M.J. Berger, P. Colella, Local adaptive mesh refinement for shock
717 hydrodynamics, *J. Comput. Phys.* 82 (1989) 64-84 doi:10.1016/0021-
718 9991(89)90035-1

- 719 [11] W.D. Henshaw, D.W. Schwendeman, Parallel computation of three-
720 dimensional flows using overlapping grids with adaptive mesh refinement,
721 J. Comput. Phys. 227 (2008) 7469-7502 doi:10.1016/j.jcp.2008.04.033
- 722 [12] S.R. Kohn, S.B. Baden, Parallel Software Abstractions for Structured
723 Adaptive Mesh Methods, J. Parallel Distrib. Comput. 61 (2001) 713-736
724 doi:10.1006/jpdc.2001.1700
- 725 [13] B.S. Kirk, J.W. Peterson, R.H. Stogner, G.F. Carey, libMesh: a C++ library
726 for parallel adaptive mesh refinement/coarsening simulations, Eng. Comput.
727 22 (2006) 237-254 doi:10.1007/s00366-006-0049-3
- 728 [14] B. van der Holst, R. Keppens, Hybrid block-AMR in cartesian and curvilinear
729 coordinates: MHD applications, J. Comput. Phys. 226 (2007) 925-946
730 doi:10.1016/j.jcp.2007.05.007
- 731 [15] A.M. Khokhlov, Fully Threaded Tree Algorithms for Adaptive Refine-
732 ment Fluid Dynamics Simulations, J. Comput. Phys. 143 (1998) 519-543
733 doi:10.1006/jcph.1998.9998
- 734 [16] P. MacNeice, K.M. Olson, C. Mobarry, R. de Fainchtein, C. Packer,
735 PARAMESH: A parallel adaptive mesh refinement community toolkit,
736 Comput. Phys. Commun., 126 (2000) 330-354 doi:10.1016/S0010-
737 4655(99)00501-9
- 738 [17] Q.F. Stout, D.L. De Zeeuw, T.I. Gombosi, C.P.T. Groth, H.G. Marshall, K.G.
739 Powell, Adaptive Blocks: A High Performance Data Structure, Proc. 1997
740 ACM/IEEE Conf. Supercomput. 57 (1997) doi:10.1109/SC.1997.10027
- 741 [18] T.H. Cormen, C.E. Leiserson, R.L. Rivest, C. Stein, Introduction to Algo-
742 rithms 2nd edition (MIT Press and McGraw-Hill, 2001)
- 743 [19] B. Hariharan, S. Aluru, Efficient parallel algorithms and software for com-
744 pressed octrees with applications to hierarchical methods, Parallel Comput.
745 31 (2005) 311-331 doi:10.1016/j.parco.2004.12.007
- 746 [20] H. Sundar, R.S. Sampath, G. Biros, Bottom-Up Construction and 2:1 Bal-
747 ance Refinement of Linear Octrees in Parallel, SIAM J. Sci. Comput. 30
748 (2008) 2675-2708 doi:10.1137/070681727

- 749 [21] C. Burstedde, L.C. Wilcox, O. Ghattas, p4est: Scalable Algorithms for Paral-
750 lel Adaptive Mesh Refinement on Forests of Octrees, *SIAM J. Sci. Comput.*
751 33 (2011) 1103-1133 doi:10.1137/100791634
- 752 [22] W. Bangerth, C. Burstedde, T. Heister, M. Kronbichler, Algorithms and
753 Data Structures for Massively Parallel Generic Finite Element Codes, *ACM*
754 *Trans. Math. Softw.* 38 (2011) 14/1-28 doi:10.1145/2049673.2049678
- 755 [23] M.S. Warren, J.K. Salmon, A Parallel Hashed Oct-Tree N-Body
756 Algorithm, *Proc. 1993 ACM/IEEE Conf. Supercomput.* (1993)
757 doi:10.1145/169627.169640
- 758 [24] R. Keppens, Z. Meliani, A.J. van Marle, P. Delmont, A. Vlasis, B.
759 van der Holst, Parallel, grid-adaptive approaches for relativistic hy-
760 dro and magnetohydrodynamics, *J. Comput. Phys.* 231 (2012) 718-744
761 doi:10.1016/j.jcp.2011.01.020
- 762 [25] A.M. Wissink, R.D. Hornung, S.R. Kohn, S.S. Smith, N. Elliott,
763 Large Scale Parallel Structured AMR Calculations Using the SAM-
764 RAI Framework, *Proc. 2001 ACM/IEEE Conf. Supercomput.* (2001)
765 doi:10.1145/582034.582040
- 766 [26] P.L. Roe, Approximate Riemann Solvers, Parameter Vectors, and Difference
767 Schemes, *J. Comput. Phys.* 43 (1981) 357-372
- 768 [27] M. Torrilhon, Uniqueness conditions for Riemann problems of
769 ideal magnetohydrodynamics, *J. Plasma Phys.* 69 (2002) 253-276
770 doi:10.1017/S0022377803002186
- 771 [28] G. Tóth, The $\nabla \cdot \mathbf{B}$ Constraint in Shock-Capturing Magnetohydrodynamics
772 Codes, *J. Comput. Phys.* 161 (2000) 605-652 doi:10.1006/jcph.2000.6519
- 773 [29] T.A. Gardiner, J.M. Stone, An unsplit Godunov method for ideal
774 MHD via constrained transport, *J. Comput. Phys.* 205 (2005) 509-539
775 doi:10.1016/j.jcp.2004.11.016
- 776 [30] T.A. Gardiner, J.M. Stone, An unsplit Godunov method for ideal MHD
777 via constrained transport in three dimensions, *J. Comput. Phys.* 227 (2008)
778 4123-4141 doi:10.1016/j.jcp.2007.12.017

- 779 [31] K. Devine, E. Boman, R. Heaphy, B. Hendrickson, C. Vaughan, Zoltan Data
780 Management Services for Parallel Dynamic Applications, *Comput. Sci. Eng.*
781 4 (2002) 90-97 doi:10.1109/5992.988653
- 782 [32] R. Diestel, *Graph Theory* 4th edition, Graduate Texts in Mathematics 173
783 (Springer-Verlag, 2010)
- 784 [33] V. Springel, *E pur si muove*, Galilean-invariant cosmological hydrodynam-
785 ical simulations on a moving mesh, *Mon. Not. R. Astron. Soc.* 401 (2010)
786 791-851 doi:10.1111/j.1365-2966.2009.15715.x
- 787 [34] R. Courant, K. Friedrichs, H. Lewy, On the partial difference equations of
788 mathematical physics, *IBM J. Res. Dev.* 11 (1967, 1928) 215-234

```

1  #include "boost/foreach.hpp"
2  #include "boost/mpi.hpp"
3  #include "cstdlib"
4  #include "vector"
5  #include "zoltan.h"
6  #define DCCRG_CELL_DATA_SIZE_FROM_USER
7  #define DCCRG_USER_MPI_DATA_TYPE
8  #include "dccrg.hpp"
9
10 struct game_of_life_cell {
11     int data[2];
12     void* at() {return &(this->data[0]);}
13     MPI_Datatype mpi_datatype() {return MPI_INT;}
14 };
15
16 int main(int argc, char* argv[]) {
17     boost::mpi::environment env(argc, argv);
18     boost::mpi::communicator comm;
19
20     float zoltan_version;
21     Zoltan_Initialize(argc, argv, &zoltan_version);
22
23     dccrg::Dccrg<game_of_life_cell> grid;
24     grid.set_geometry(10, 10, 1, 0, 0, 0, 1.0, 1.0, 1.0);
25     grid.initialize(comm, "HYPERGRAPH", 1, 0);
26     grid.balance_load();
27     const std::vector<uint64_t> cells = grid.get_cells();
28
29     // initial state
30     BOOST_FOREACH(const uint64_t cell, cells) {
31         game_of_life_cell* cell_data = grid[cell];
32         cell_data->data[0] = cell_data->data[1] = 0;
33         if (cell % 4 == 0) cell_data->data[0] = 1;
34     }
35
36     for (int turn = 0; turn < 10; turn++) {
37         grid.update_remote_neighbor_data();
38
39         // collect live neighbor counts
40         BOOST_FOREACH(const uint64_t cell, cells) {
41             game_of_life_cell* cell_data = grid[cell];
42             cell_data->data[1] = 0;
43
44             const std::vector<uint64_t>* neighbors = grid.get_neighbors(cell);
45             BOOST_FOREACH(const uint64_t neighbor, *neighbors) {
46                 if (neighbor == dccrg::error_cell) continue;
47                 game_of_life_cell* neighbor_data = grid[neighbor];
48                 if (neighbor_data->data[0] == 1) cell_data->data[1]++;
49             }
50         }
51         // assign new state
52         BOOST_FOREACH(const uint64_t cell, cells) {
53             game_of_life_cell* cell_data = grid[cell];
54             if (cell_data->data[1] == 3) cell_data->data[0] = 1;
55             else if (cell_data->data[1] != 2) cell_data->data[0] = 0;
56         }
57     }
58     return 0;
59 }

```

Figure 4: A complete parallel program playing Conway's Game of Life using dccrg, see the text for details.

```

1  struct Cell {
2      unsigned int number_of_particles;
3      std::vector<boost::array<double, 3> > particles;
4      static bool transfer_particles;
5
6      // returns the starting address of data to send/receive
7      void* at() {
8          if (Cell::transfer_particles) {
9              if (this->particles.size() > 0) {
10                 return &(this->particles[0]);
11             } else {
12                 // return a sane address
13                 return &(this->number_of_particles);
14             }
15         } else {
16             return &(this->number_of_particles);
17         }
18     }
19
20     // returns the length in bytes to send/receive
21     MPI_Datatype mpi_datatype() const {
22         MPI_Datatype datatype;
23         if (Cell::transfer_particles) {
24             MPI_Type_contiguous(
25                 this->particles.size() * sizeof(boost::array<double, 3>),
26                 MPI_BYTE, &datatype);
27         } else {
28             MPI_Type_contiguous(1, MPI_UNSIGNED, &datatype);
29         }
30         return datatype;
31     }
32
33     void resize() {
34         this->particles.resize(this->number_of_particles);
35     }
36 }; // struct Cell
37
38 int main(...) {
39     dccrg::Dccrg<Cell> grid;
40     ...
41     for (int step = 0; step < max_steps; step++) {
42         // update number of particles between processes
43         Cell::transfer_particles = false;
44         grid.update_remote_neighbor_data();
45
46         // allocate space for particles in copies of remote neighbors
47         const boost::unordered_set<uint64_t>* remote_neighbors
48             = grid.get_remote_cells_with_local_neighbors();
49         BOOST_FOREACH(const uint64_t remote_neighbor, *remote_neighbors) {
50             Cell* data = grid[remote_neighbor];
51             data->resize();
52         }
53
54         // update particle data between processes
55         Cell::transfer_particles = true;
56         grid.update_remote_neighbor_data();
57     }
58 }

```

Figure 5: Relevant excerpts from a simple kinetic simulation showing how to use dccrg when the amount of data in grid cells varies both in space and in time, see text for details.

Scalability of MHD in meteo

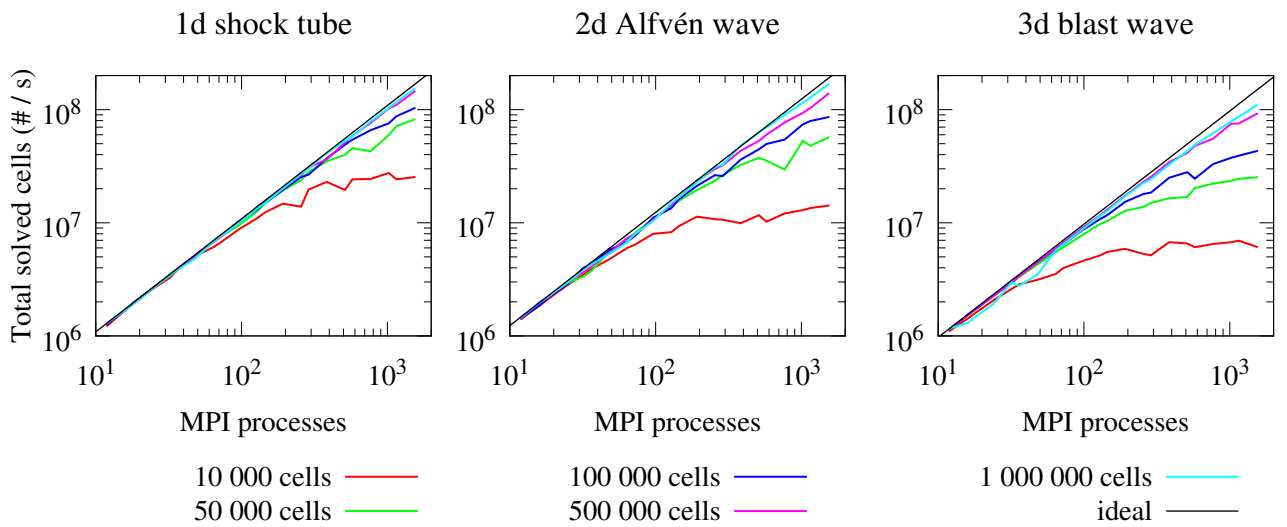


Figure 6: Strong MHD scalability tests results with a static grid in one, two and three dimensions in Meteo (Cray XT5m). Total number of solved cells per second is shown as a function of the number of processes used and the total number of cells in each simulation. Ideal line is extrapolated from the 12 process result with 1 M cells.

Static grid blast wave profile

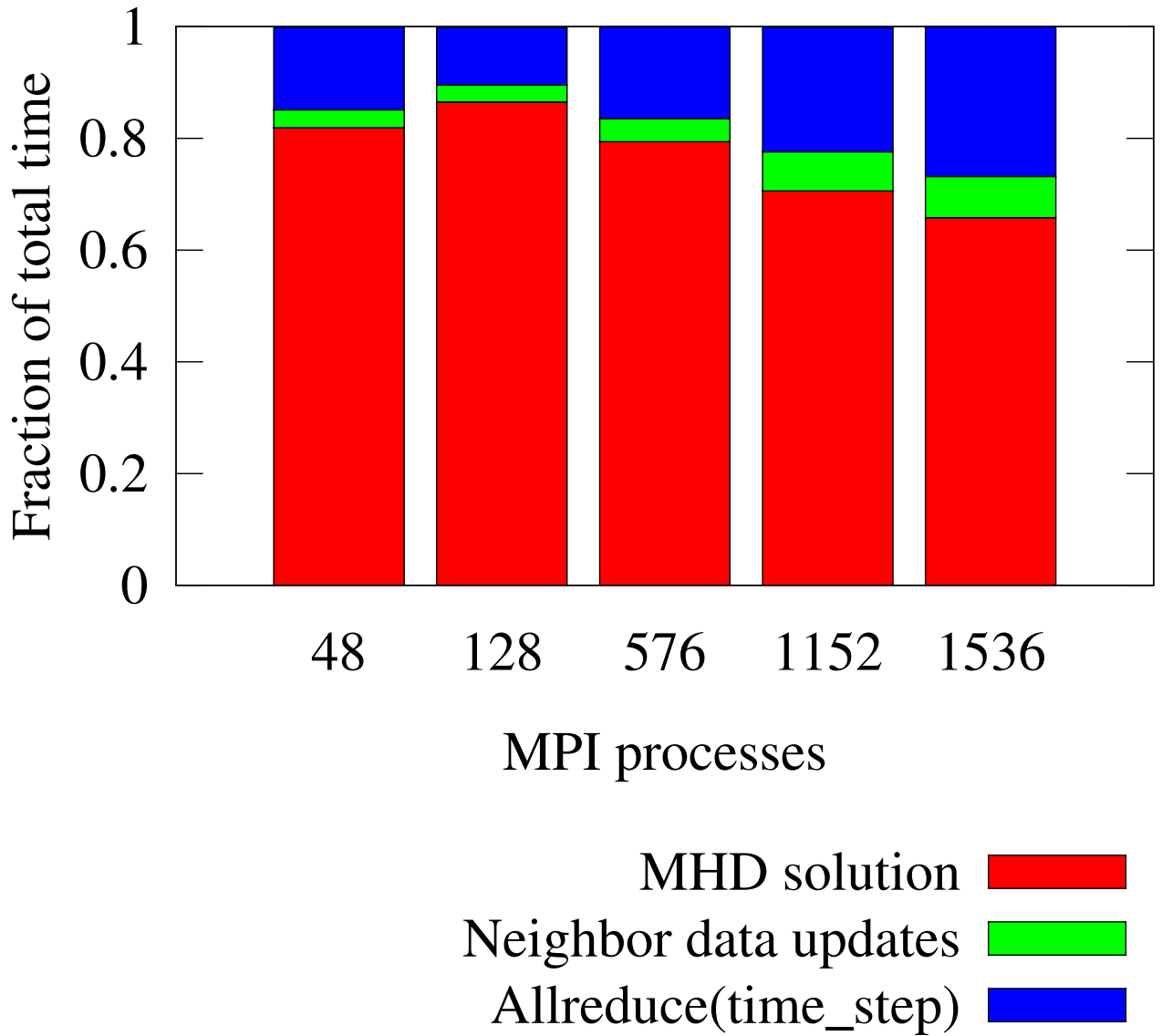


Figure 7: Profile of the three dimensional MHD blast wave test without AMR using 1 M cells. Allreduce labels the only global communication executed each time step where the maximum length of the physical time step is obtained using MPI_Allreduce. Initialization and file I/O are not included.

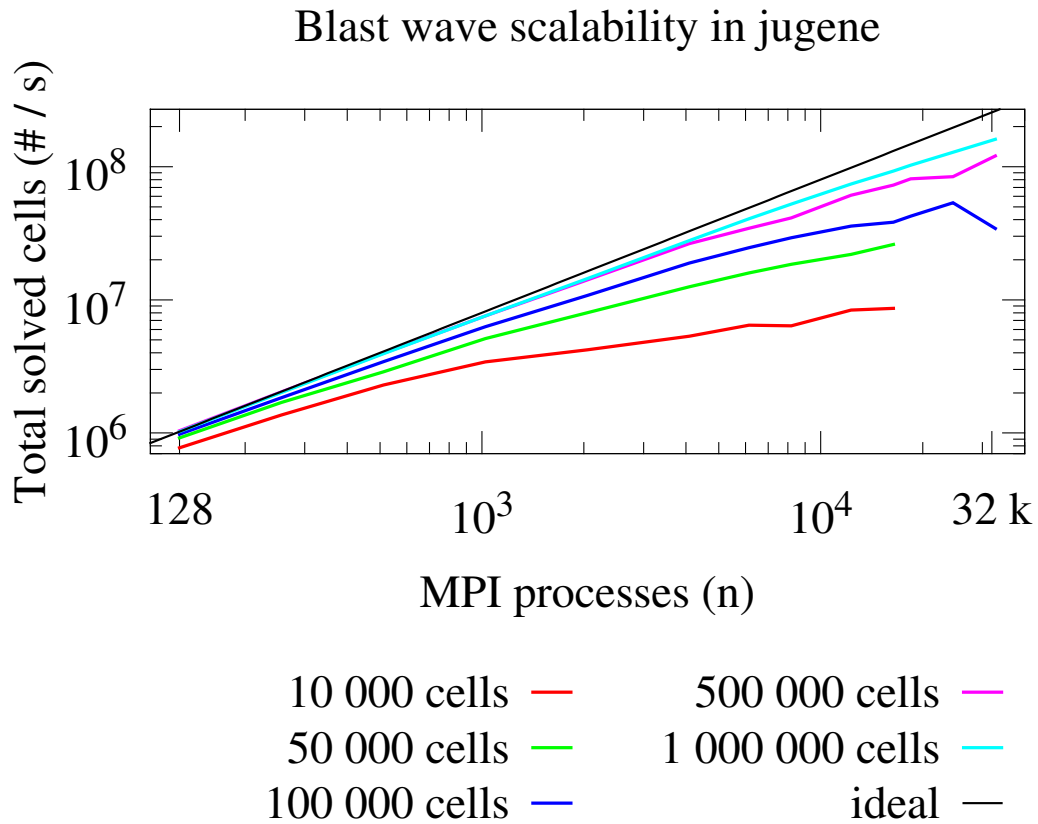


Figure 8: Strong MHD scalability tests results with a static grid in three dimensions in Jugene (IBM Blue Gene/P). Total number of solved cells per second is shown as a function of the number of processes used and the total number of cells in each simulation. Ideal line is extrapolated from the 128 process result with 1 M cells.

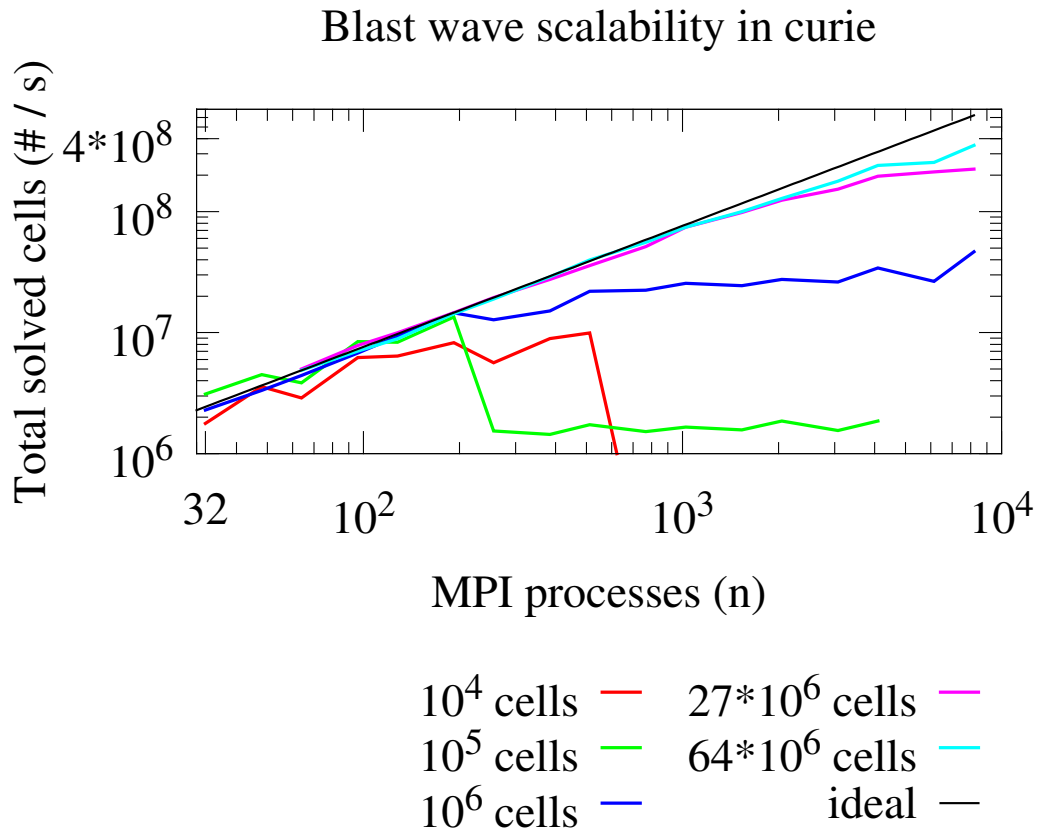


Figure 9: Strong MHD scalability tests results with a static grid in three dimensions in Curie (bullx InfiniBand). Total number of solved cells per second is shown as a function of the number of processes used and the total number of cells in each simulation. Ideal line is extrapolated from the 32 process result with 64 M cells.

Speed of pure adaptive mesh refinement

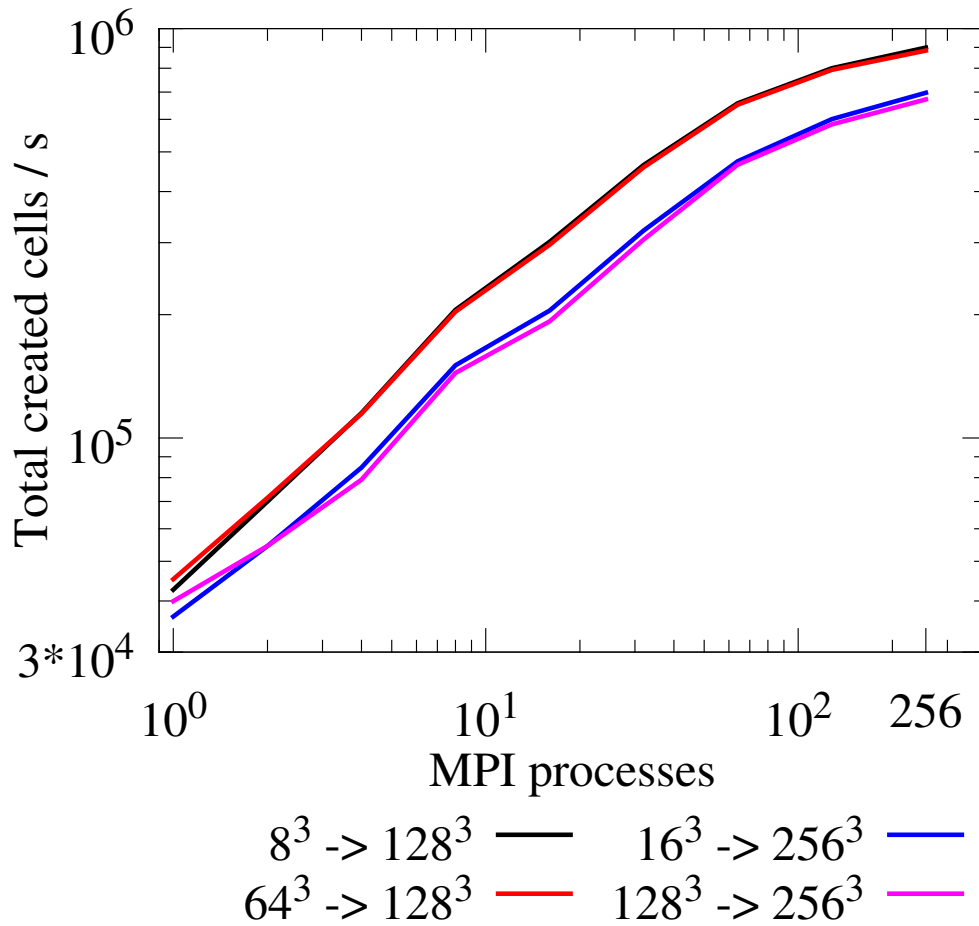


Figure 10: Speed of adaptive mesh refinement in dccrg. Initial size of the grid is 8^3 , 16^3 , 64^3 or 128^3 cells. Every process refines each local cell until the total size of the grid is 128^3 or 256^3 cells.

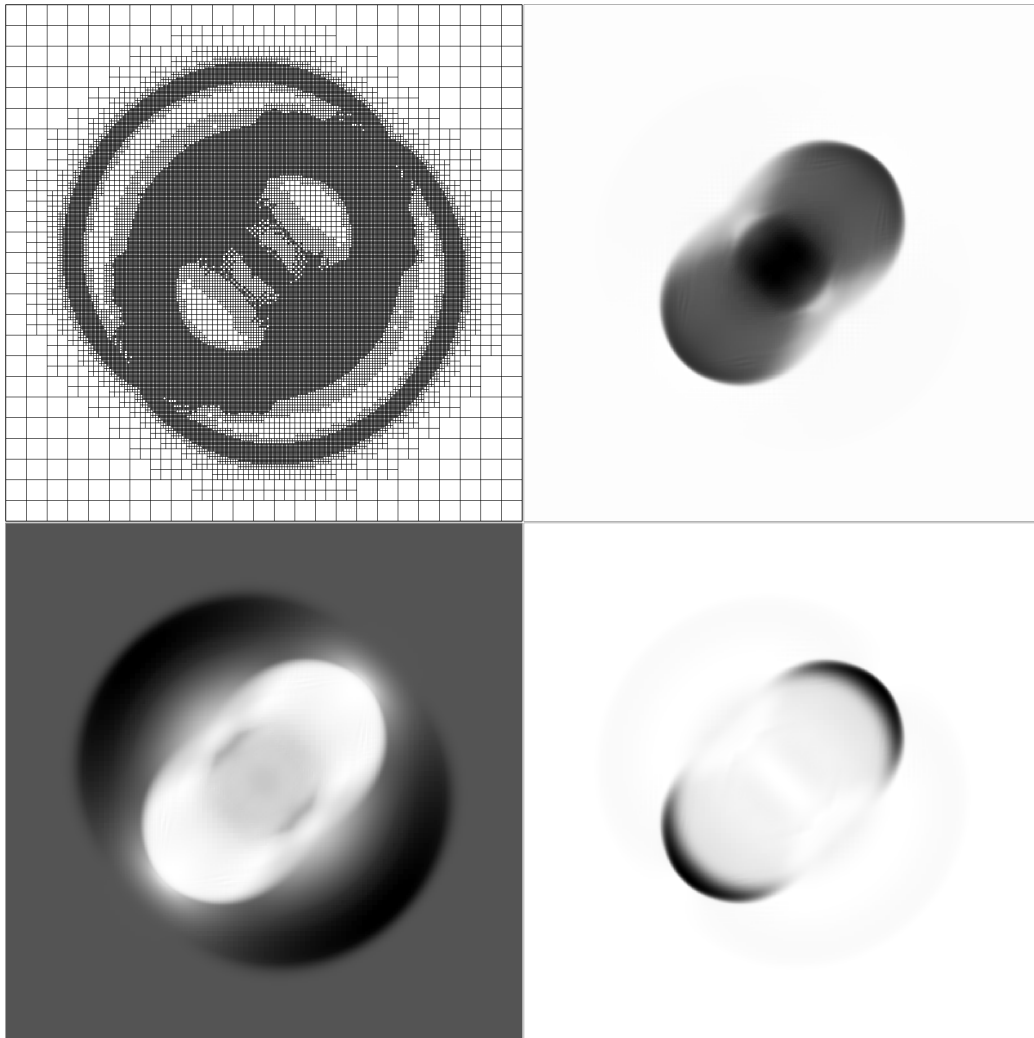


Figure 11: Adaptive mesh refinement used in a MHD blast wave test (from [30]) showing from left to right, top to bottom the grid, pressure, magnetic and kinetic energy density during the simulation (final state of simulation in the print version) in the $y = 0$ plane when grid is adapted at every time step. At the end of the simulation the fraction of maximum to minimum values are 15 for density (not shown), 43 for pressure and 2.3 for magnetic energy density.

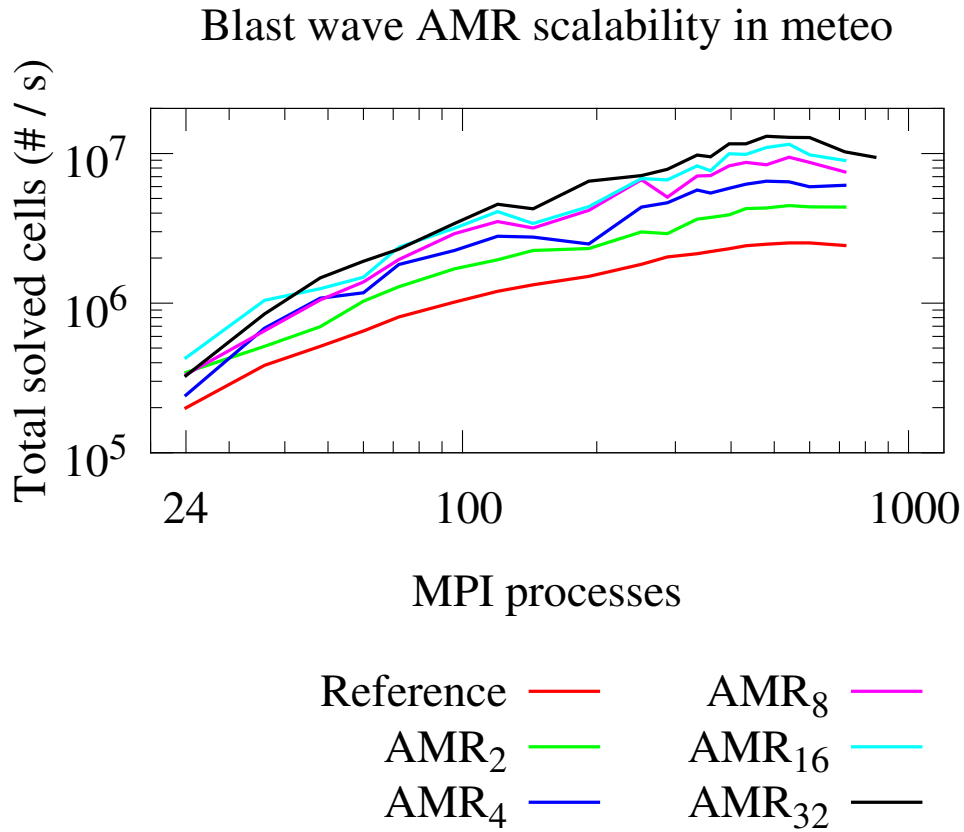


Figure 12: Scalability of adaptive mesh refinement used in a MHD blast wave test ([30]). In the reference run a CFL of 0.4 is used, AMR is done at every time step and the load is balanced whenever the local cell fraction f_c exceeded 2, where $f_c = N_{max}/N_{min}$ and max and min are the maximum and minimum number of local cells among processes respectively. The AMR_N runs are otherwise identical to the reference run but CFL is set to $0.4/N$ and AMR is done every Nth time step, essentially multiplying the amount of non-AMR work in these runs by N.

Run-time AMR blast wave profile

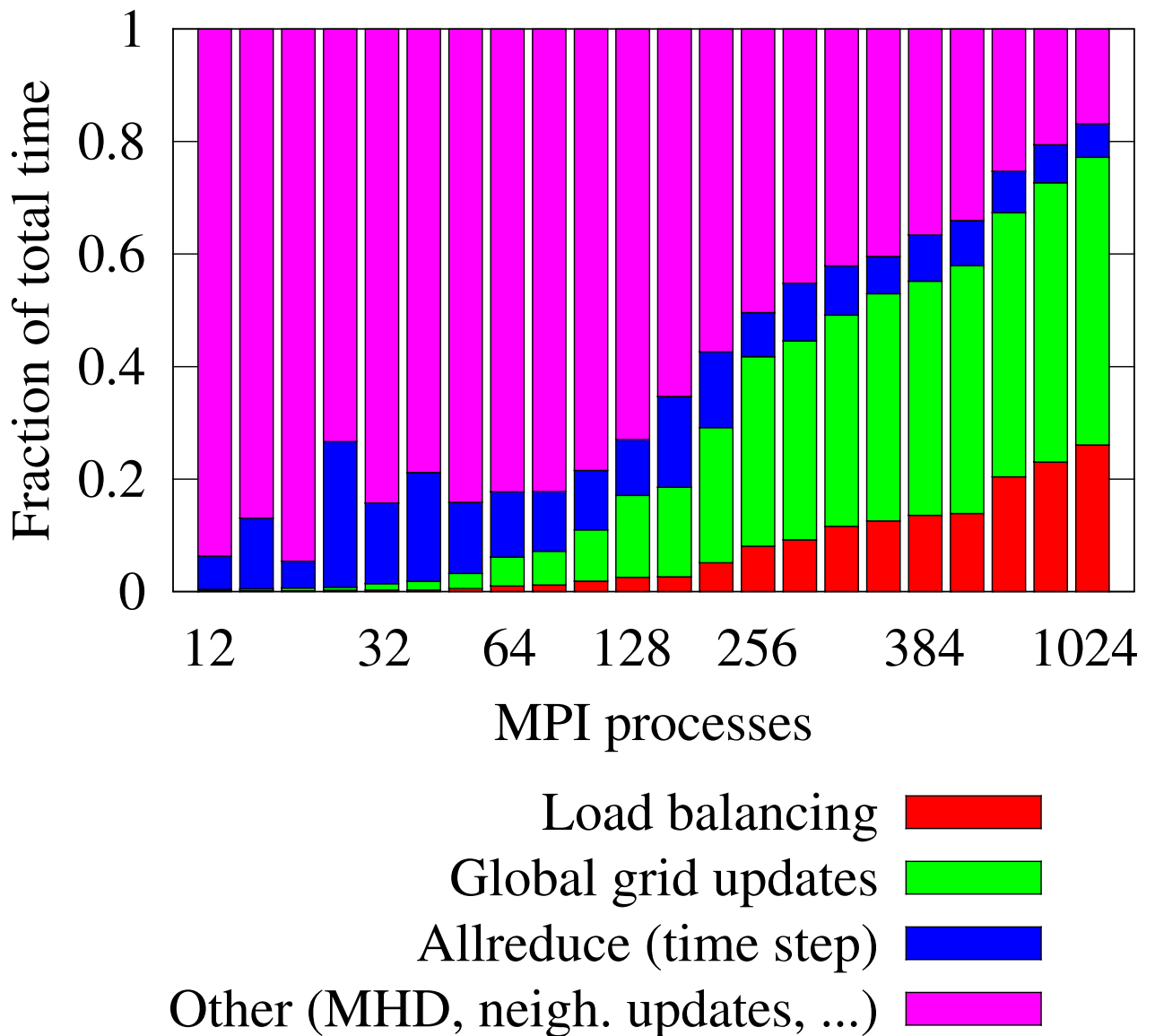


Figure 13: Profile of the three dimensional MHD blast wave test with AMR using at most 10 M cells. Allreduce labels the calculation of the maximum length of the physical time step obtained using MPI_Allreduce. Initialization and file I/O are not included.